# Plasmonic Nanopowders for Photothermal Therapy of Tumors

**ARTICLE** *in* LANGMUIR · MARCH 2012

Impact Factor: 4.46 · DOI: 10.1021/la300022k · Source: PubMed



**6 AUTHORS**, INCLUDING:

Boris Khlebtsov
Russian Academy of Sciences
**153** PUBLICATIONS **2,192** CITATIONS
SEE PROFILE

George S Terentyuk
Saratov State University
**47** PUBLICATIONS **491** CITATIONS
SEE PROFILE

Andrey Valentinovich Ivanov
N.N. Blokhin Cancer Research Center
**25** PUBLICATIONS **176** CITATIONS
SEE PROFILE

Nikolai G. Khlebtsov
Institute of Biochemistry and Physiology of Pl…
**229** PUBLICATIONS **4,828** CITATIONS
SEE PROFILE

Langmuir

Article

pubs.acs.org/Langmuir

# Plasmonic Nanopowders for Photothermal Therapy of Tumors

Boris N. Khlebtsov,[†] Elizaveta V. Panfilova,[†] Georgy S. Terentyuk,[‡] Irina L. Maksimova,[‡] Andrei V. Ivanov,[§] and Nikolai G. Khlebtsov*[,†,‡]

[†]Institute of Biochemistry and Physiology of Plants and Microorganisms, Russian Academy of Sciences, 13 Prospekt Entuziastov, Saratov 410049, Russia

[‡]Saratov State University, 83 Ulitsa Astrakhanskaya, Saratov 410026, Russia

[§]Blokhin Russian Cancer Research Center, 24 Kashirskoe Shosse, Moscow 115478, Russia

Supporting Information

**ABSTRACT:** We describe a novel strategy for the fabrication of plasmonic nanopowders (dried gold nanoparticles) by using wet chemical nanoparticle synthesis, PEG-SH functionalization, and a standard freeze-drying technique. Our strategy is illustrated by successful fabrication of different plasmonic nanopowders, including gold nanorods, gold−silver nanocages, and gold nanospheres. Importantly, the dried nanoparticles can be stored for a long time under usual conditions and then can easily be dissolved in water at a desired concentration without such hard manipulations as sonication or heating. Redispersed samples maintain the plasmonic properties of parent colloids and do not form aggregates. These properties make pegylated freeze-dried gold nanoparticles attractive candidates for plasmonic photothermal therapy in clinical settings. In this work, redispersed gold nanorods were intravenously administered to mice bearing Ehrlich carcinoma tumors at doses of 2 and 8 mg (Au)/kg (animal). Particle biodistribution was measured by atomic absorption spectroscopy, and tumor hyperthermia effects were studied under laser NIR irradiation. Significant tumor damage was observed only at the higher dose of the nanorods.

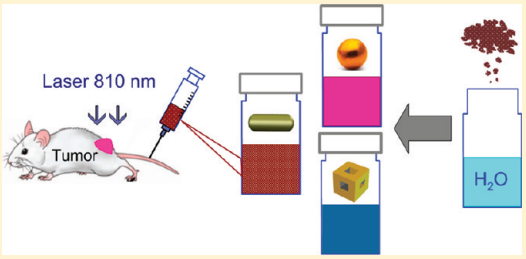


## INTRODUCTION

Plasmonic photothermal therapy (PPT) of tumors is a promising trend in current nanomedicine[1] that utilizes selective laser heating of accumulated nanoparticles. Different types of nanoparticles have been reported as suitable candidates for PPT in vitro and in vivo, including silica/gold nanoshells,[2−5] gold nanorods (GNRs),[6−9] and gold−silver nanocages.[10−12] In general, PPT efficiency is determined by several factors,[13,14] including (1) selective accumulation of particles in a tumor, owing to the enhanced permeability and retention (EPR) effect[15] or owing to active targeting;[16] (2) effective and selective tumor heating, owing to spatial localization and spectral selectivity of particles as light-to-heat transducers because of the spectral tuning of plasmonic absorption to the tissue transparency window;[17] (3) optimization of therapy protocols in respect to particle administration doses, delivery of light irradiation to targets, and effective control over particle distribution, localization, and heating to achieve the desired thermolysis outcome.[13,14]

In the context of optimal PPT particles, GNRs have the advantages of being easy to prepare with a desired longitudinal NIR resonance and with a smaller size at least in one dimension in comparison with silica/gold nanoshells and nanocages. As a rule, for in vivo PPT, one uses intravenous injection of PEG-coated GNRs[9,18] in order to increase the EPR effect (through the enhanced circulation lifetime of particles in blood) and to decrease interference with immune cells such as macrophages,[14] owing to the stealth effect.[19,20]

Active targeting is a rare exception at present[21] because of its unclear efficiency in improving the accumulation contrast in tumors. For example, it has been reported recently[22] that the conjugation of GNRs to three different tumor-specific ligands only marginally improves total particle accumulation in tumors in comparison with PEG-coated particles, whereas intracellular and extracellular nanoparticle distribution can be greatly affected. This means that if the total accumulation contrast is the primary goal, the usual PEG-coated particles can be used for PPT treatment.

Despite the evident progress in the development of PPT, there are no clinically approved pharmaceuticals on the market, except for one product, based on pegylated gold nanoshells, which has been commercialized by Nanospectra Biosciences and is in the process of FDA-sanctioned human studies.[23] Along with some concerns related to the biodistribution and potential biotoxicity of nanoparticles,[24] the existing strong barriers to the transfer of laboratory PPT protocols to clinics include such technological issues as particle storage and

**Special Issue:** Colloidal Nanoplasmonics

**Received:** January 3, 2012
**Revised:** March 9, 2012
**Published:** March 11, 2012

   dx.doi.org/10.1021/la300022k | *Langmuir* 2012, 28, 8994−9002

sterilization under usual conditions, accurate determination of dosages, and usability. For instance, commercially available GNRs are coated with the highly toxic cetyltrimethylammonium bromide (CTAB), whereas biofunctionalized GNRs (Ntraker)[25] are supplied by the manufacturer as suspensions with a limited keeping time and with concentrations in terms of optical density. In typical synthesis protocols,[7] the mass−volume concentrations lie in the range of 50−100 mg/L, whereas successful PPT can be achieved at higher concentrations of injected samples (up to 400 mg/L).[9] Thus, in the context of clinical PPT applications, there is an obvious need in a powder alternative instead of colloid formulations of plasmonic nanoparticles. The ultimate goal is to design convenient technologies for the fabrication of stable and water-soluble nanopowders that would retain all physicochemical and optical properties of the parent functionalized colloidal particles but could be stored for a long time under usual conditions and could easily be dissolved on application in water or PBS at a desired concentration. Beyond just PPT applications, there has been great interest in the fabrication of nanorod-based SERS substrates for chemical and biological sensing,[26] and plasmonic nanorod powders could also be used in this field.

The fabrication of nanoparticle powders from parent colloids is not a new approach. In particular, colloidal gold nanospheres were prepared in powder form for particles coated with dodecylamine,[27] *Aspergillus niger*,[28] and poly(2-(methacryloyloxy)ethyl phosphorylcholine).[29] Hainfeld et al.[30] reported fabrication of a powder consisting of 1.9 nm pegylated gold nanospheres approved by the FDA for intravenous injection as an X-ray contrast agent. However, gold nanospheres have limited efficiency for PPT because of their weak absorption in NIR and their too short wavelength plasmonic resonance near 520 nm. Honda et al.[31] obtained a gold nanorod powder by functionalization of particles with 6-amino-1-hexanethiol. It was shown that the powder can be dissolved in water after being stored at −80 °C for several months. Quite recently, Zubarev and co-workers[32] fabricated gold nanorod powders by lyophilization of colloidal particles covered with (16-mercaptohexadecyl)trimethylammonium bromide (MTAB). The MTAB-covered GNRs were shown to be nontoxic and were also efficiently taken up by cancer cells in vitro in very large amounts, in comparison with the control pegylated particles.

Here, we describe fabrication of gold nanorod powders that are especially suitable for PPT applications. The nanorod-powder protocol was also used for successful fabrication of dry pegylated gold nanospheres and gold−silver nanocages. To the best of our knowledge, the powder gold−silver nanocages have been fabricated in this work for the first time. According to our preliminary observations, all nanopowders retain their properties for at least 6 months under usual conditions, and they can easily be dissolved in water or PBS at a desired concentration without sonication or heating. All the end user needs to do is add water or PBS to a desired weight of powder and shake the solution slightly in a matter of seconds. To assess the utility of dry GNRs for PPT, we used a xenografted mouse tumor model and NIR laser irradiation after intravenous injection of redispersed particles.

## EXPERIMENTAL SECTION

**Materials.** The following reagents were used: $AgNO_3$ (>99.9%; Aldrich, 20.913-9); cetyl trimethylammonium bromide (96%, Fluka, no. 52370); tetrachloroauric acid ($HAuCl_4$, >99%; Sigma-Aldrich); isoascorbic acid (AsA, >99%, Fluka); sodium borohydride (Sigma-Aldrich); hydrochloric acid (chemical grade, Vekton Co., Russia); $K_2C0_3$ (chemical grade, Reakhim Co., Russia); mPEG-SH (Nektar Therapeutics, MW5000); ethylene glycol (EG) (99%, Aldrich; 293237); poly(vinyl pyrrolidone) (PVP) ($M_w$ = 55 000, Sigma-Aldrich, 85.656-8); a 30% aqueous solution of ammonia (Aldrich); acetone (analytical grade, Vekton Co., Russia); absolute ethanol (99.99%, Scharlau, 64-17-5); $Na_2S{\cdot}9H_2O$ (chemical grade, GOST 2053-77); condensed argon (99.99%); sodium citrate (Sigma, 99%); and Milli-Q water (18 MΩ × cm, Millipore).

**Fabrication of Nanoparticles and Powders.** GNRs were fabricated by a seed-mediated method following Nikoobakht and El-Sayed,[33] with minor modifications.[34] Briefly, a seed solution was obtained by mixing 10 mL of 0.1 M CTAB and 250 μL of 10 mM $HAuCl_4$, followed by adding 1 mL of ice-cold 10 mM $NaBH_4$. The seeds were aged for 2 h. GNRs were obtained by mixing 900 mL of 0.1 M CTAB, 50 mL of 10 mM $HAuCl_4$, 20 mL of 4 mM $AgNO_3$, 10 mL of 0.1 M AsA, 10 mL of 1 M HCl, and 10 mL of the seed solution. The mixture was aged at 30 °C for 48 h until an orange-red suspension was formed. Thereby, we obtained 1 L of GNR solution with the longitudinal plasmon resonance at 820 nm and a total gold concentration of 85 mg/L.

Along with GNRs, quasispherical colloidal gold particles with an average diameter of 56 nm were synthesized by the Frens method,[35] and 48 nm gold−silver nanocages were fabricated by the method of Skrabalak et al.,[36] with minor modifications[37] (see the Supporting Information).

GNR solutions were centrifuged twice at 16 000*g* for 1 h and were redispersed in water to remove an excess of CTAB molecules. The pH of the GNR solutions was adjusted to 9 by addition of 0.2 M $K_2CO_3$, followed by addition of mPEG-SH at a final concentration of 10 nM. The mixture was allowed to react overnight. Pegylated rods were centrifuged at 16 000*g* for 60 min and were redispersed in water to remove nonspecifically bound PEG molecules. The pegylated GNRs were again centrifuged at 16 000*g* for 1 h and redispersed in a small amount of water to a concentration of 5 g/L. To completely remove CTAB and unreacted PEG, the nanoparticles were dialyzed against water for 72 h with several replacements of water. Finally, these dialyzed, pegylated, and concentrated GNRs were transferred to a sterile bottle, frozen in liquid nitrogen, and freeze-dried overnight under vacuum.

In our pegylation of CTAB-coated GNRs, we followed the protocol described by Liao and Hafner.[38] By using Raman spectra, those authors showed the absence of CTAB on the particle surface after the displacement of the CTAB bilayer by mPEG-SH molecules. According to our observations, PEG-coated GNR powders can easily be dispersed in ethanol and isopropyl alcohol, whereas CTAB-coated GNRs aggregate in these solvents. Further evidence for the absence of CTAB toxicity of freeze-dried GNRs comes from an MTT assay, as described in the Supporting Information (section S7).

Similar protocols were also used to fabricate colloidal gold and gold−silver nanocage powders, but the centrifugation regimens were adjusted accordingly (see the Supporting Information).

**In Vivo Laser Hyperthermia.** For PPT experiments, female Balb/c mice (Stolbovaya Nursery of the Russian Academy of Sciences; age, 3 months; weight, 20−22 g) were used. Before and during the experiment, the animals were maintained according to the European Convention for the Protection of Vertebrate Animals used for Experimental and Other Scientific Purposes.[39] For statistical averaging, two experimental groups of 14 animals and two control groups of 6 animals were selected randomly.

A xenografted tumor model was obtained by intramuscular injection of Ehrlich carcinoma cells (0.2 mL, $1.2 \times 10^6$ cells/mL) into the left mouse flank. By the 14th day after injection, the average tumor volume was 0.5 ± 0.2 $cm^3$ (Supporting Information Figure S6). For in vivo experiments, the nanorod powder was redispersed in a 0.9% NaCl solution to concentrations of 100 and 400 mg/L immediately before administration to animals. For animals of the first and second experimental groups (bearing Ehrlich carcinoma tumors), pegylated


dx.doi.org/10.1021/la300022k | *Langmuir* 2012, 28, 8994−9002

GNRs were administered at doses of 2 and 8 mg (Au)/kg (animal), respectively (0.4 mL at concentrations of 100 and 400 mg/L). The control animals were injected with 0.4 mL of saline buffer. Thus, the average total doses of injected Au were 40 and 160 $\mu$g.

Twenty-four h after injection of the particles, photothermal measurements were made with tumors and symmetrically located healthy tissues, which were epilated before laser irradiation at 810 nm (LIMO semiconductor diode laser, Dortmund, Germany). Animals of both experimental and control groups were irradiated in a CW regimen for 5 min at 4 W/cm$^2$. The second control group was intact. One h after irradiation, seven animals from each experimental group were sacrificed, and muscle, spleen, liver, and tumor tissues were sampled for biodistribution analysis. The other seven animals of each experimental group and four animals of each control group were used for survival control. The two remaining mice of the control groups were also used for biodistribution control measurements.

**Measurements.** Absorbance spectra were acquired by using a Specord 250 BU UV−visible-NIR spectrometer (Analytik Jena, Germany). Transmission electron microscopy (TEM) images of nanoparticles were obtained using a Libra-120 microscope (Carl Zeiss, Germany). The gold and silver percentages in the tissue samples were determined by atomic absorption spectroscopy with a Dual Atomizer Zeeman AA spectrometer, iCE 3500 (Thermo Scientific Inc.). To calibrate the atomic absorption spectrometer (AAS) for quantitative analysis of Au, we used two procedures. In the first one, the AAS was calibrated by using a $HAuCl_4$ solution in 0.1 M HCl. In the second method, we used a gold (15 nm) colloid with known Au content, as determined from citrate reduction of $HAuCl_4$. The colloid was treated by adding an aqua regia ($3HCl/1HNO_3$) mixture. Both calibration procedures gave consistent data within 10% experimental error. An IR thermograph, IRISYS 4010 (InfraRed Integrated System Ltd., U.K.), was used for noninvasive monitoring of surface tissue temperatures. The zeta potential of the particles before and after drying was measured with a Zetasizer Nano-ZS instrument (Malvern, U.K.).

## RESULTS AND DISCUSSION

**Nanorod Powder.** Figure 1 shows general scheme and the experimental procedures used for the fabrication of pegylated nanorod powders. To stress some critical steps, two failed routes are also shown.

As-prepared GNR solutions (Figure 1A) were tested by TEM and extinction spectra measurements. According to Figure 2, GNR particles resemble, in general, cylinders with semispherical ends; and subtle deviations from cigarlike shape (related to the flat end-cap and "dog bone" morphologies[34]) are small for this sample. From TEM images of 500 particles, the average length and diameter are $L$ = 41.1 ± 8.5 nm and $d$ = 10.2 ± 1.9 nm, respectively. The inset in Figure 2a shows the number distribution of the particles, $\Delta N_i/\Delta r_i$, over aspect ratios $r_i = L_i/d_i$ with an average value $r$ = 4.03 ± 0.7. A typical extinction spectrum of gold nanorods (panel b, curve 1) is shown in terms of the extinction coefficient $\mu_{ext} = \ln(10)A_{ext}/l$ (cm$^{-1}$), where $A_{ext}$ is the measured extinction (absorption + scattering) and $l$ is the layer thickness. Theoretical spectrum 2 was calculated by using a T-matrix solvable model for non-cigarlike rods and a TEM-based statistical ensemble consisting of 500 particles and byproduct particles (3.5%), as described in detail elsewhere.[34] For comparison, the absolute maxima of the measured and calculated spectra were equated (8.2 cm$^{-1}$ at 820 nm), and for size-dependent correction of the gold dielectric function, the surface electron scattering constant was taken to be 1/3.[34]

The as-prepared sample was centrifuged at 16 000$g$ for 60 min to give a dark-red sediment of concentrated CTAB-coated nanoparticles (Figure 1B). It should be emphasized that concentrated pellets of CTAB-coated particles cannot be used for nanopowder fabrication. This is indicated by a red-crossed arrow in Figure 1B. Indeed, both room-temperature vacuum drying and freeze-drying give similar products: dark brown nanopowders (Figure 1C). Unfortunately, these powders consist of aggregated particles, and after the addition of water they give light-purple suspensions with visible flocs (Figure 1D). Although these flocs can be redispersed under intense continuous sonication, the extinction spectra of redispersed CTAB-coated powders reveal strong distortions and deviations from the parent colloid spectrum (see Supporting Information Figure 1S). These deviations clearly indicate the presence of aggregates, which can be seen in the TEM images (Supporting Information Figure 2Sb). Furthermore, the redispersed CTAB-

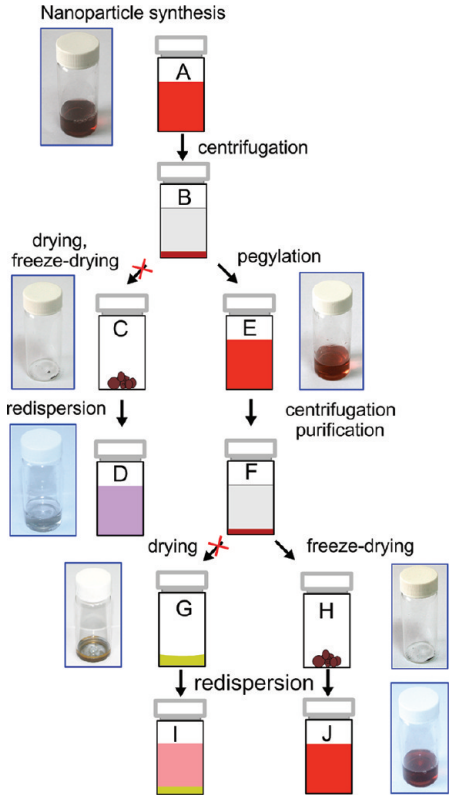


**Figure 1.** Schematic illustration of the experimental procedures used for GNR powder fabrication. Two failed routes are marked by red crosses.

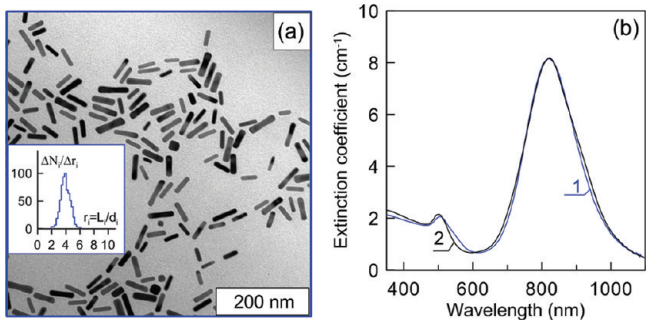


**Figure 2.** TEM images (a) and experimental extinction spectrum (b, curve 1) of an as-prepared GNR suspension with an extinction coefficient of 8.2 cM$^{-1}$ at a plasmon resonance wavelength of 820 nm. The inset in panel (a) shows the aspect ratio distribution. Curve 2 was calculated by the T-matrix method by using a TEM-based statistical ensemble of rods, as described in ref 34.


dx.doi.org/10.1021/la300022k | Langmuir 2012, 28, 8994−9002

coated GNRs were unstable, and they aggregated within 1 day. Thus, CTAB-coated GNRs are not suitable for freeze-drying and one needs an alternative functionalization of GNRs by molecules preventing GNR aggregation. This is the first critical step of nanopowder fabrication.

After pegylation (Figure 1E), washing, and concentration of GNRs (Figure 1F), the pellet with pegylated GNRs was treated by two standard techniques: (1) room-temperature vacuum drying (Figure 1G) and (2) freeze-drying (Figure 1H). In the first case, an aureate film formed (Figure 1G), similar to that observed previously by Honda et al.[31] for GNRs stabilized by 6-amino-1-hexanethiol. In agreement with that work,[31] our aureate film also could be redispersed in water immediately after drying, and the extinction spectrum of the redispersed sample was close to that of the parent colloid. However, the GNR yield (as determined from the resonance maximum) was not complete, and it decreased in the course of time. Specifically, the GNR yield was equal to 80% immediately after drying, but after room-temperature storage for a week, the percentage of redispersed GNRs decreased to 20%. Furthermore, after 1 week storage, the aureate film was strongly adhered to the vial wall, making further work quite inconvenient and resulting in additional loss of particles. Thus, room-temperature drying is the second failed route of powder fabrication (marked by a crossed arrow between the F and G steps in Figure 1).

Subsequent freeze-drying of the pegylated GNR pellet produced a dark-brown powder (Figure 1H) that was much dense than the fluffy powder obtained in ref 32 after lyophilization of MTAB-coated GNRs. The fabricated powder of PEG-coated GNRs can easily be transferred to vessels, weighed, and dissolved in water or PBS without additional procedures (Figure 1J and Figure 3e–g). Extinction spectroscopy and TEM analysis of the redispersed and parent GNR colloids did not reveal any differences (Figure 3a,b and Supporting Information Figure 2Sc,d). Our preliminary observations suggest that the storage of powders at room temperature for 6 months does not lead to changes in their plasmonic properties or to any decrease in the GNR yield, which exceeds 95% (Figure 3a). In the Supporting Information, we provide a video file illustrating convenient work with the fabricated powder, including its transfer from the storage vessel for weighing, redispersion in water, and spectral measurements.

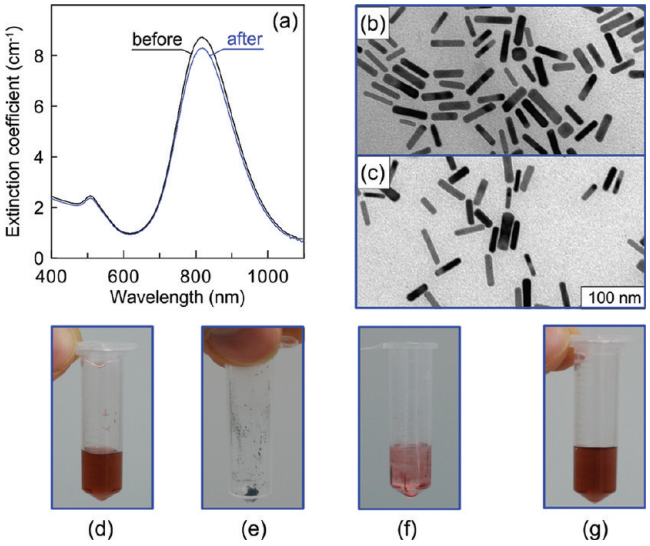


**Figure 3.** Extinction spectra (a) and TEM images of GNRs before freeze-drying (b) and after redispersion in water (c). Bottom photos show as-prepared pegylated GNRs (d), the freeze-dried powder (e), the solution immediately after the addition of water (f), and the GNR colloid after gentle shaking for several seconds (g).

Looking at the drying and freeze-drying routes after step F in Figure 1, we conclude that the observed difference in the GNR yield and water solubility between the final products (formed from the same parent colloids) may have been caused by the different structures of the aureate film and the dark-brown powder. It seems reasonable to suggest that an easy penetration of water between the powder particles ensures its complete redispersion, whereas the aureate film is formed by a densely packed particle monolayer with a poor penetration of water through the glass/air/film boundary. To confirm this hypothesis, we placed a drop of pegylated GNRs directly onto a TEM grid and performed the drying and freeze-drying treatments. In full agreement with our assumption, TEM analysis revealed a fractal-like porous structure after freeze-drying and a dense monolayer after room-temperature drying (Figure 4).

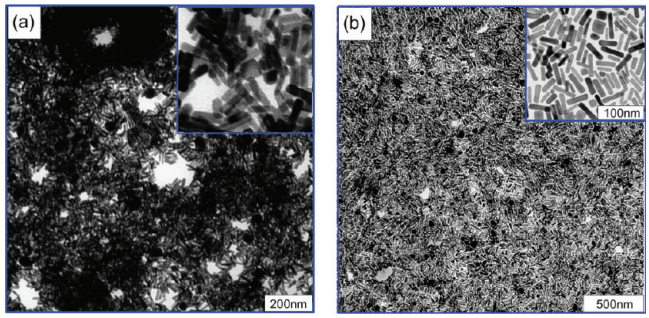


**Figure 4.** TEM images of a porous fractal-like (a) and a dense monolayer-like (b) structure formed after freeze-drying (a) and room-temperature drying (b) of a drop of pegylated GNRs placed directly on a TEM grid.

It is interesting to note that, after repeated purification and freeze-drying, GNRs did not aggregate and could be redispersed easily. It is known that as-prepared GNRs retain their colloidal stability when the CTAB concentration is diluted to 2–10 mM. This property is often used to remove an excess of CTAB by a single centrifugation and redispersion in water. However, subsequent centrifugation and redispersion results in irreversible aggregation of GNRs because of the completely lost electrostatic stabilization, related to the positive charge of the CTAB bilayer. During GNR synthesis and the formation of the CTAB bilayer, the negative net charge of the "bare" particles is reversed and the effective zeta-potential of CTAB-coated nanorods becomes positive. Pegylation of GNRs leads to replacement of CTAB with PEG-SH molecules, which are electrically neutral or may be slightly negative owing to $OH^-$ groups (depending on pH). Therefore, pegylation of GNRs effectively restores the initial negative charge of the "bare" particles, thus making the effective zeta-potential of the PEG-coated nanorods negative (see below, Table 1). In general, electric repulsion and steric factor stabilize PEG-coated particles; however, it is the steric factor, not the electric one, which makes main contribution to particle stability and allows


dx.doi.org/10.1021/la300022k | Langmuir 2012, 28, 8994–9002

**Table 1. Zeta Potentials of the As-Prepared Particles and Those Redispersed from Powders**

| pegylated particles | zeta potential before drying (mV) | zeta potential after redispersion of dried powders (mV) |
|---|---|---|
| gold nanorods | −18.7 ± 2.0 | −19.2 ± 2.0 |
| gold nanospheres | −22.5 ± 2.5 | −24.7 ± 2.5 |
| gold−silver nanocages | −32.5 ± 3.0 | −31.7 ± 3.0 |

multiple purification steps of PEG-coated nanorods without aggregation.

**Colloidal Gold and Gold−Silver Nanocage Powders.** Pegylation of gold nanoparticles with PEG-SH is a routine and universal procedure that could be applied to various particle types, including colloidal gold particles, silica/gold nanoshells, gold−silver nanocages, and so on. As pegylation and freeze-drying are two basic steps of GNR powder fabrication, the same nanopowder protocol can be applied to other particles as well. In this work, we chose colloidal gold nanospheres and gold−silver nanocages as illustrative examples. The synthesis and characterization of these particles are described in detail in the Supporting Information (sections S3 and S4). The only difference between fabrication of GNR powders and fabrication of colloidal gold and Au−Ag nanocage powders consists of centrifugation conditions (in this case, 10 000*g* for 20 min). Figure 5a,b shows the extinction spectra of CG particles before and after freeze-drying and redispersion, together with photos of the corresponding colloids. Clearly, the optical properties of the redispersed colloid are close to those of the parent sample. TEM analysis also confirmed identity of both samples. Similar data are shown in Figure 5c,d for Au−Ag nanocages.

Additional evidence for the preservation of physicochemical properties of the dried particles came from zeta potential ($\zeta$) measurements. According to Table 1, there were no significant differences in $\zeta$ values between the parent colloids and their powder counterparts, whereas the absolute $\zeta$ values depended on the particle type.

**In Vivo Laser Hyperthermia.** Using GNR powders, we prepared two stock solutions with concentrations of 100 and 400 mg/L for intravenous injection of 0.4 mL per mouse. The corresponding administered doses were 2 and 8 mg (Au)/kg (animal), corresponding to the most popular dose range of 1−10 mg/kg, used in biodistribution and toxicity experiments with gold nanoparticles.[24] It should be noted that the published data[24] revealed no toxicity of gold nanoparticles in a short-time (about 1 week) cure, with the daily administration dose being less than 0.5 mg/kg. Thus, our doses lay within these toxicity limits or were a bit higher. On the other hand, in a successful PPT experiment with xenografted mouse tumor models,[9] the GNR administered doses were significantly higher (about 20 mg/kg).

Figure 6 shows GNR biodistribution for two doses (2 and 8 mg/kg) and for four organs: tumor, healthy muscle tissue, liver, and spleen. In general, the ratio between the amounts of accumulated gold in all organs roughly corresponded to the ratio of administered doses, 2:8 = 1:4, whereas the gold content in the control samples was significantly lower than that in the experimental samples. In agreement with numerous literature data,[24] the gold accumulation in the liver and spleen was about 1 order higher than that in the tumors, and the total gold content accounted for about 10% of the administered gold. Similarly to the data by Akiyama et al.[40] for a close xenografted model in vivo, our data show enhanced accumulation of GNRs

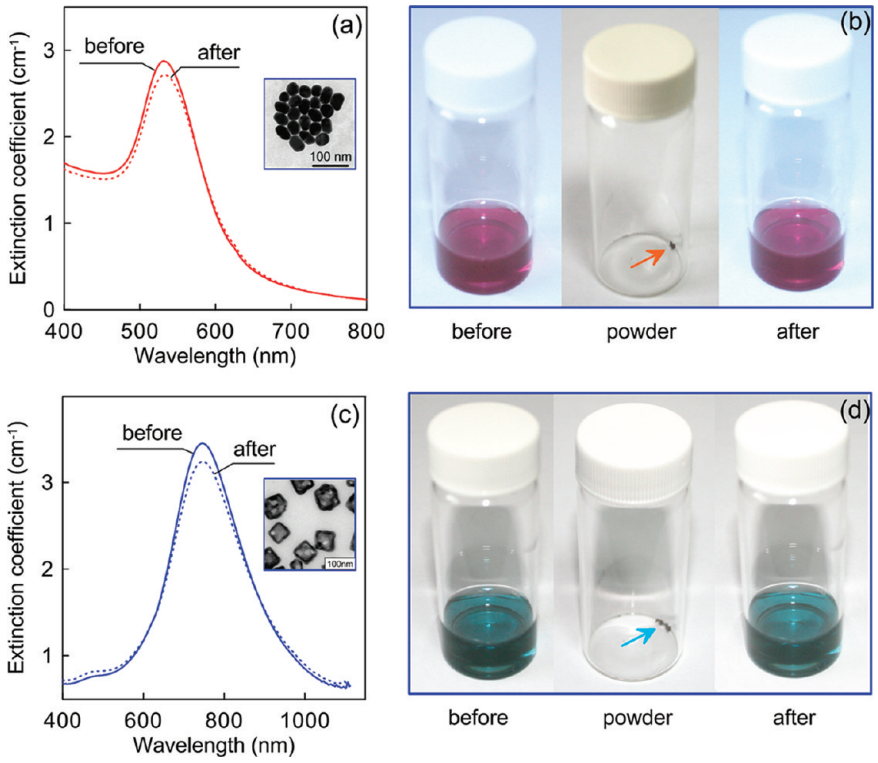


**Figure 5.** Extinction spectra of colloidal gold (a) and gold−silver nanocages (c) before and after freeze-drying. Photos (b) show vials with an as-prepared CG solution (left), freeze-dried powder (center, indicated by an arrow), and redispersed CG particles (right). Similar photos are shown in row (d) for Au−Ag nanocages.


dx.doi.org/10.1021/la300022k | *Langmuir* 2012, 28, 8994−9002

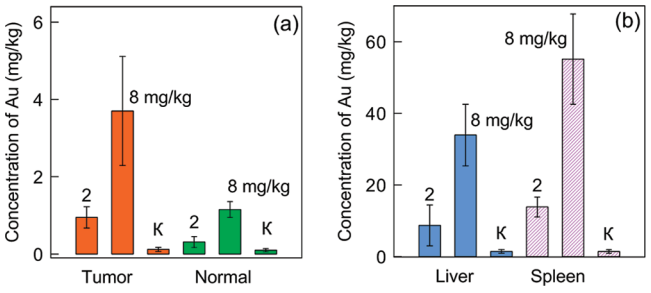


**Figure 6.** Biodistribution of GNRs in terms of the accumulated gold concentration in the tumor and normal tissue (a) and in the liver and spleen (b). Measurements were made by AAS at 24 h after injection of redispersed GNR powders at doses of 2 and 8 mg/kg. The symbol κ stands for the control group after the injection of saline buffer without Au nanoparticles.

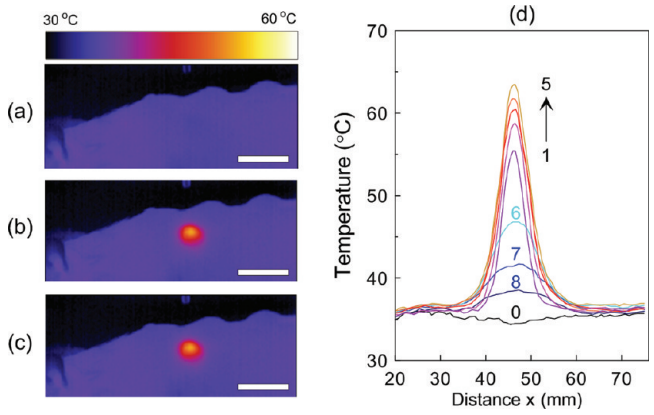


**Figure 7.** 2D temperature distribution on the tumor surface before laser irradiation (a) and 1 min (b) and 5 min (c) after the beginning of the irradiation. In vivo measurements were made at 24 h after intravenous GNR injection at a dose of 8 mg (Au)/kg (animal). The scale bar is 10 mm, and the black area is outside the tissue (blue). Panel (d) shows the temperature distribution along the horizontal *x*-direction within a laser spot before irradiation (0), 1−5 min after the switch-on of CW laser irradiation (810 nm, 4 W/cm$^2$, the laser beam diameter is 6 mm, curves 1−5), and 1−3 min after the switch-off of the laser (curves 6−8, respectively).

in the spleen, as compared with that in the liver. Note that the total accumulation of gold in liver (about 35 mg/kg) and spleen (about 55 mg/kg) was several times higher than the administered doses of 2 and 8 mg/kg. Taking into account the typical weights of the mouse liver and spleen (Balb/c, 1.1 and 0.1 g, respectively),[41] the total accumulation of gold in both organs was about 40 mg or 25% of the total administered gold (160 mg). This result is in reasonable agreement with the data of Akiyama et al.[40] for GNRs and with other literature data on gold nanoparticle biodistribution.[24] Although the gold concentration in the liver (in terms of mg/kg) was somewhat lower than that in the spleen, in toto, the absolute gold content in the liver was higher because of the larger organ mass.

The gold content in the tumor amounted to about 1% of the injected gold concentrations, exceeding the average values for healthy tissues by three or four times. In other words, the gold content per unit weight of tumor was 1 mg/kg and 4 mg/kg for the two administered doses, 2 mg/kg and 8 mg/kg, respectively. Evidently, this was driven mostly by the enhanced uptake by tumors, owing to the enhanced permeability and retention (EPR) effect.[15] Thus, even passive accumulation of pegylated GNRs, without conjugation of particles to targeting biomolecules, results in an evident accumulation contrast at a level of 5% of the total injected gold. The obtained data are in general agreement with other reports on the biodistribution and passive tumor accumulation of pegylated gold nanoparticles.[40,42]

Figure 7 shows IR thermography data in terms of 2D temperature distributions under NIR laser irradiation of the tumor at 24 h after the intravenous injection of GNRs. According to the data of Figure 7, the spatial temperature distribution over laser spots is inhomogeneous because of the inhomogeneous distribution of the incident intensity and owing to heat redistribution from hot to cold regions. PPT efficiency is determined not only by the maximal laser spot temperature, but also by the overall dimension of the region in which the temperature exceeds the hyperthermia or thermolysis limits (45−47 °C). In our experiment (Figure 7d), the average diameter of a hot spot (>45 °C) was equal to 7 mm at 1 min after the beginning of the laser irradiation and to 11 mm after 5 min. It is clear that in our case the heated area is determined by the laser beam diameter. Accordingly, many accumulated particles and, possibly, their aggregates contribute to the average temperature rise. This case is different from the single-particle heating of microcapsules by laser pulses, in which the temperature rise takes place over the characteristic size of a heating object.[43]

Figure 7d shows detailed spatial temperature distributions along the horizontal *x*-coordinate, passing through the laser spot center. The first five curves in Figure 7d were recorded each at 1 min after the laser switch-on, and the other three curves illustrate tumor cooling after the laser switch-off.

In general, these curves are consistent with intuitive expectations based on a consideration of heating and thermal diffusion processes. However, surprisingly enough, we observed more efficient heating of tissues as compared to heating of water suspensions possessing equivalent GNR concentrations. A possible explanation is that the concentration of GNRs accumulated in the tumor periphery is higher than that in the tumor core. A similar effect was reported by Chen et al.[12] for a biodistribution and histological examination of tumors with accumulated gold−silver nanocages. A more detailed discussion of this point will be presented elsewhere.[44]

The temperature versus time curves in Figure 8 were obtained from the central point of plots similar to Figure 7d and were averaged over seven experimental mice (curves 1 and 2). Curves 3 represent controls for normal tissues without GNR injection. Evidently, the main temperature increase took place during the first 100 s, and then the heating rate decreased. Even for the lower injected dose of 2 mg/kg (Figure 8a), we observed a notable difference between laser heating of the tumor and that of the neighboring normal tissue. Under steady-state conditions, the temperature increment was about 10 °C. In the case of control animals without GNR injection, our thermographic measurements did not reveal any significant differences between the surface temperatures of the tumorous and healthy tissues. However, at 24 h after intravenous injection of the lower GNR dose (2 mg/kg), the temperature increment for healthy muscle tissues was about 5 °C because of the small accumulation of GNRs in those tissues. In the case of intravenous injection of the higher GNR dose (8 mg/kg), the passive accumulation of GNRs in tumors resulted in strong temperature contrast (about 30 °C), in comparison with the


dx.doi.org/10.1021/la300022k | Langmuir 2012, 28, 8994−9002

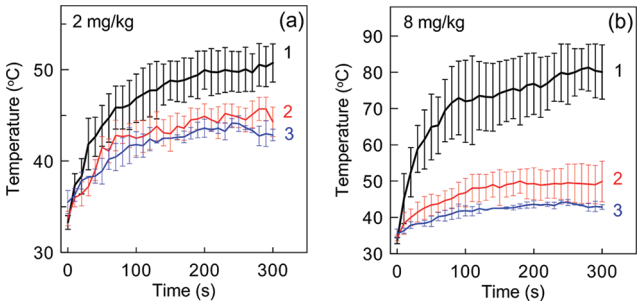


**Figure 8.** Time-dependent laser heating of tumorous (1) and normal (2) tissues at 24 after GNR injection at 2 (a) and 8 (b) mg/kg. Curves 3 show the kinetics of laser heating of normal tissue for the control group without nanoparticle injection. All data were recorded at the center of the laser spot at 5 min after the beginning of irradiation and were averaged over the animals of the experimental and control groups.

temperature of the neighboring healthy tissue of the same animal. As early as 1−2 min after laser irradiation, the tumor temperature approached 70 °C, whereas it was only 50 °C for the lower dose of 2 mg/kg.

Figure 9 shows survival data after PPT treatment in terms of tumor volume plotted over time. Tumor growth was followed

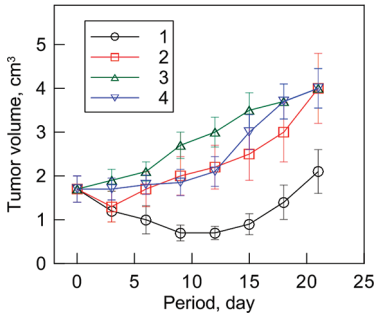


**Figure 9.** Tumor volumes at different times after PPT. 1 and 2 are experimental groups, which received injection of GNRs at 8 (1) and 2 (2) mg/kg. 3 and 4 are the control groups, with laser irradiation but without nanoparticle injection (3) and without all treatments (4).

by serially measuring tumor dimensions in two orthogonal directions twice weekly and calculating the tumor volume using an approximation by spheroid shape. As illustrated in Figure 9, there was a statistically significant difference in tumor growth delay in the case of laser hyperthermia combined with the higher dose of injected GNRs (8 mg/kg, curve 1). Under these experimental conditions, there was significant thermodestruction of tumors, resulting in a 2-fold decrease in tumor volume. However, there also remained undamaged regions over the tumor periphery that eventually gave recessive growth. In the case of the lower injected dose of GNRs, the growth delay was minimal. Interestingly, in the case of control group 3, the laser irradiation of the tumors and their heating up to 40 °C even resulted in stimulated tumor growth instead of a delay, in agreement with other observations.[45,46]

## CONCLUSIONS

We have fabricated three types of plasmonic nanopowders consisting of freeze-dried pegylated GNRs, gold−silver nanocages, and colloidal gold nanospheres. These nanopowders have been stored at our laboratory under the usual room-temperature conditions for almost 6 months without any change in their initial (as-prepared) properties. Specifically, the freeze-dried PEG-coated particles can easily be dissolved in water or PBS buffer at a desired concentration in a matter of seconds without sonication or heating.

Two important notes are in order here. First, one can assume that our approach can also be used for the fabrication of nanopowders consisting of more sophisticated conjugates, prepared by using various PEG-SH derivatives and small target molecules. In particular, we have fabricated colloidal gold nanopowders conjugated to folic acid by using the PEG-SH linker. However, according to our preliminary data, these dried particles cannot be stored for a long time. Second, we noted progressive deterioration of water solubility of nanopowders with an increase in the particle size. In particular, we failed to fabricate acceptable nanopowders by using parent colloids of silica/gold nanoshells with outer diameters of about 140−160 nm. Thus, further work is needed to fix these problems.

Although we have demonstrated the experimental PPT of a xenografted tumor only with the GNR powder, other plasmonic powders can also be used for the same purposes. For example, Chen et al.[12] demonstrated irreversible damage to tumor cells and a decrease in metabolic tumor activity in the case of PPT with intravenous nanocage injection and laser exposure. The use of colloidal gold nanopowders for PPT can be justified by two effects that are not related directly to NIR plasmonic heating of individual nanospheres, whose resonance lies near 520−530 nm. First, the clusterization of nanospheres within the tumor cells shifts their collective resonance to NIR, thus making PPT with NIR lasers possible. Second, the overall plasmonic heating is not the sole effect determining the effectiveness of PPT.[47] Rapid heating of nanoparticles under laser irradiation can produce vapor bubbles,[48] which can cause cavitation damage to cells irradiated with visible[49] or NIR[50] light. Thus, cavitation damage can be an additional or synergetic effect to particle-enhanced absorption hyperthermia.

Considering the data of Figure 9, we believe that GNR-mediated mild-temperature hyperthermia may not be effective. In light of the previously reported data,[9] a more useful PPT strategy can be based on the use of high administered doses, which induces tumor-specific localized vascular disruption/collapse and extensive tissue necrosis. Further, the GNR-mediated hyperthermia can enhance the efficacy of other therapeutic treatments (see, e.g., the combination of gold nanoshell-mediated hyperthermia and radiation therapy).[51]

One serious PPT problem is the undesired distribution and accumulation of gold nanoparticles after intravenous injection. Indeed, it is well established now[24] that all organs of the reticuloendothelial system (in particular, liver and spleen) are the basic primary target for accumulation of gold nanoparticles within the size range of 10−100 nm (see Figure 6). Active targeting of GNPs by TNF-$\alpha$[52] or by other tumor-specific peptide ligands[22] does not significantly improve GNP biodistribution; in any case, the Au content in the liver and spleen is still greater than that in the tumor. As the excretion of accumulated particles from the liver and spleen can take up to 3−4 months,[52] the questions as to the injected doses, possible inflammation processes, and nanoparticle excretion and clearance are still of great importance. Whereas little toxicity has been observed upon in vivo administration of PEG-coated GNRs, further long-term toxicological investigations and new strategies to facilitate hepatobiliary clearance are clearly needed in order to accelerate the translation of PPT technologies to


dx.doi.org/10.1021/la300022k | Langmuir 2012, 28, 8994−9002

clinics.[53] In particular, as the undesired accumulation of gold nanoparticles is caused by systemic administration, direct intratumoral injection may be the preferred route of plasmonic nanoparticle administration. Another possible solution may be GNR administration via the "isolated limb perfusion",[54] a medical technique used to deliver anticancer drugs (e.g., AurimuneCYT-6091[55]) directly to an arm or a leg. In this method, the flow of blood to and from the limb is temporarily stopped with a tourniquet while an anticancer drug is administered.

Finally, it would be very interesting to examine the new functionalization approach suggested by Zubarev and co-workers[32] for MTAB-coated GNRs for in vivo PPT applications. Provided that the reported in vitro dramatic increase in cellular particle uptake[32] gives a similar tumor accumulation contrast without strong correlation with immune cells and RTE organ accumulation, it would be a breakthrough step toward the PPT of cancer.

## ■ ASSOCIATED CONTENT

### Supporting Information

Extinction spectra of CTAB-coated GNRs before and after freeze-drying; TEM images of CTAB-coated and PEG-coated GNRs before and after freeze-drying; protocols for the synthesis of silver nanocubes, gold−silver nanocages, and colloidal gold particles, together with extinction spectra and TEM images; an implanted Ehrlich carcinoma tumor image; the toxicity study of powder PEG-coated GNRs using MTT assay with HeLa cells; the video file "GNR-PEG-SH-Powder.wmv", illustrating convenient work with the fabricated GNR powder. This material is available free of charge via the Internet at http://pubs.acs.org.

## ■ AUTHOR INFORMATION

### Corresponding Author

*E-mail: khlebtsov@ibppm.sgu.ru.

### Notes

The authors declare no competing financial interest.

## ■ ACKNOWLEDGMENTS

This work was supported by the Russian Foundation for Basic Research, by grants from the President and the Ministry of Education and Science of the Russian Federation (MK-1057.2011.2, Contract No. 14.740.11.260), and by a grant from the Government of the Russian Federation designed to support scientific research projects implemented under the supervision of leading scientists at Russian institutions of higher education. We thank N. I. Polyanskaya (Cancer Research Center, RAMS), A. M. Burov, O. A. Bibikova, S. A. Staroverov, and V. A. Khanadeev (IBPPM RAS) for help with TEM and MTT, and D. N. Tychinin (IBPPM RAS) for his help in preparation of the manuscript.

## ■ REFERENCES

(1) Dreaden, E. C.; Alkilany, A. M.; Huang, X.; Murphy, C. J.; El-Sayed, M. A. The Golden Age: Gold Nanoparticles for Biomedicine. *Chem. Soc. Rev.* **2012**, DOI: 10.1039/c1cs15237h.

(2) O'Neal, D. P.; Hirsch, L. R.; Halas, N. J.; Payne, J. D.; West, J. L. Photo-Thermal Tumor Ablation in Mice Using Near Infrared-Absorbing Nanoparticles. *Cancer Lett.* **2004**, *209*, 171−176.

(3) Loo, C.; Lowery, A.; Halas, N. J.; West, J. L.; Drezek, R. Immunotargeted Nanoshells for Integrated Cancer Imaging and Therapy. *Nano Lett.* **2005**, *5*, 709−711.

(4) Bardhan, R.; Lal, S.; Joshi, A.; Halas, N. Theranostic Nanoshells: From Probe Design to Imaging and Treatment of Cancer. *Acc. Chem. Res.* **2011**, *44*, 936−946.

(5) Terentyuk, G. S.; Maslyakova, G. N.; Suleymanova, L. V.; Khlebtsov, N. G.; Khlebtsov, B. N.; Akchurin, G. G.; Maksimova, I. L.; Tuchin, V. V. Laser-Induced Tissue Hyperthermia Mediated by Gold Nanoparticles: Toward Cancer Phototherapy. *J. Biomed. Opt.* **2009**, *14*, 021016(1−9).

(6) Huang, X. H.; El-Sayed, I. H.; Qian, W.; El-Sayed, M. A. Cancer Cell Imaging and Photothermal Therapy in the Near-Infrared Region by Using Gold Nanorods. *J. Am. Chem. Soc.* **2006**, *128*, 2115−2120.

(7) Murphy, C. J.; Gole, A. M.; Stone, J. W.; Sisco, P. N.; Alkilany, A. M.; Goldsmith, E. C.; Baxter, S. C. Gold Nanoparticles in Biology: Beyond Toxicity to Cellular Imaging. *Acc. Chem. Res.* **2008**, *41*, 1721−1730.

(8) Huang, X.; Neretina, S.; El-Sayed, M. A. Gold Nanorods: From Synthesis and Properties to Biological and Biomedical Applications. *Adv. Mater.* **2009**, *21*, 4880−4910.

(9) von Maltzahn, G.; Park, J. H.; Agrawal, A.; Bandaru, N. K.; Das, S. K.; Bhatia, S. N. Computationally Guided Photothermal Tumor Therapy Using Long-Circulating Gold Nanorod Antennas. *Cancer Res.* **2009**, *69*, 3892−3900.

(10) Chen, J.; Wang, D.; Xi, J.; Au, L.; Siekkinen, A.; Warsen, A.; Li, Z.-Y.; Zhang, H.; Xia, Y.; Li, X. Immuno Gold Nanocages with Tailored Optical Properties for Targeted Photothermal Destruction of Cancer Cells. *Nano Lett.* **2007**, *7*, 1318−1322.

(11) Au, L.; Zheng, D.; Zhou, F.; Li, Z. Y.; Li, X.; Xia, Y. A Quantitative Study on the Photothermal Effect of Immuno Gold Nanocages Targeted to Breast Cancer Cells. *ACS Nano* **2008**, *2*, 1645−1652.

(12) Chen, J.; Glaus, C.; Laforest, R.; Zhang, Q.; Yang, M.; Gidding, M.; Welch, M. J.; Xia, Y. Gold Nanocages as Photothermal Transducers for Cancer Treatment. *Small* **2010**, *6*, 811−817.

(13) Kennedy, L. C.; Bickford, L. R.; Lewinski, N. A.; Coughlin, A. J.; Hu, Y.; Day, E. S.; West, J. L.; Drezek, R. A. A New Era for Cancer Treatment: Gold-Nanoparticle-Mediated Thermal Therapies. *Small* **2011**, *7*, 169−183.

(14) Dykman, L. A.; Khlebtsov, N. G. Gold Nanoparticles in Biomedical Applications: Recent Advances and Perspectives. *Chem. Soc. Rev.* **2012**, *41*, 2256−2282.

(15) Iyer, A. K.; Khaled, G.; Fang, J.; Maeda, H. Exploiting the Enhanced Permeability and Retention Effect for Tumor Targeting. *Drug Discovery Today* **2006**, *11*, 812−818.

(16) Llevot, A.; Astruc, D. Applications of Vectorized Gold Nanoparticles to the Diagnosis and Therapy of Cancer. *Chem. Soc. Rev.* **2011**, *41*, 242−257.

(17) Khlebtsov, B.; Zharov, V.; Melnikov, A.; Tuchin, V.; Khlebtsov, N. Optical Amplification of Photothermal Therapy with Gold Nanoparticles and Nanoclusters. *Nanotechnology* **2006**, *17*, 5167−5179.

(18) Kogan, B. Y.; Andronova, N. V.; Khlebtsov, N. G.; Khlebtsov, B. N.; Rudoy, V. M.; Dement'eva, O.; Sedykh, E.; Bannykh, L. Pharmacokinetic Study of Pegylated Plasmon Resonant Gold Nanoparticles in Tumor-Bearing Mice. *NSTI Nanotech 2008, Nanotechnol. Conf. Trade Show, Tech Proc.* **2008**, *2*, 65−68.

(19) Niidome, T.; Yamagata, M.; Okamoto, Y.; Akiyama, Y.; Takahashi, H.; Kawano, T.; Katayama, Y.; Niidome, Y. PEG-Modified Gold Nanorods with a Stealth Character for *in Vivo* Applications. *J. Controlled Release* **2006**, *114*, 343−347.

(20) Wang, L.; Li, Y. F.; Zhou, L.; Liu, Y.; Meng, L.; Zhang, K.; Wu, X.; Zhang, L.; Li, B.; Chen, C. Characterization of Gold Nanorods *in Vivo* by Integrated Analytical Techniques: Their Uptake, Retention, and Chemical Forms. *Anal. Bioanal. Chem.* **2010**, *396*, 1105−1114.

(21) Li, Z.; Huang, P.; Zhang, X.; Lin, J.; Yang, S.; Liu, B.; Gao, F.; Xi, P.; Ren, Q.; Cui, D. RGD-Conjugated Dendrimer-Modified Gold Nanorods for *in Vivo* Tumor Targeting and Photothermal Therapy. *Mol. Pharmaceutics* **2010**, *7*, 94−104.

(22) Huang, X.; Peng, X.; Wang, Y.; Wang, Ya.; Shin, D. M.; El-Sayed, M. A.; Nie, S. A Reexamination of Active and Passive Tumor

Targeting by Using Rod-Shaped Gold Nanocrystals and Covalently Conjugated Peptide Ligands. *ACS Nano* **2010**, *4*, 5887−5896.
(23) http://nanospectra.com/technology/aurolasetherapy.html.
(24) Khlebtsov, N.; Dykman, L. Biodistribution and Toxicity of Engineered Gold Nanoparticles: a Review of *in Vitro* and *in Vivo* Studies. *Chem. Soc. Rev.* **2011**, *40*, 1647−1671.
(25) http://nanopartz.com/Gold_Nanorods.htm.
(26) Alvarez-Puebla, R. A.; Liz-Marzán, L. M. Traps and Cages for Universal SERS Detection. *Chem. Soc. Rev.* **2011**, *41*, 43−51.
(27) Swami, A.; Kumar, A.; Sastry, M. Formation of Water-Dispersible Gold Nanoparticles Using a Technique Based on Surface-Bound Interdigitated Bilayers. *Langmuir* **2003**, *19*, 1168−1172.
(28) Bhambure, R.; Bule, M.; Shaligram, N.; Kamat, M.; Singhal, R. Extracellular Biosynthesis of Gold Nanoparticles Using *Aspergillus niger* − its Characterization and Stability. *Chem. Eng. Technol.* **2009**, *32*, 1036−1041.
(29) Yuan, J.-J.; Schmid, A.; Armes, S. P.; Lewis, A. L. Facile Synthesis of Highly Biocompatible Poly(2-(methacryloyloxy)-ethylphosphorylcholine)-Coated Gold Nanoparticles in Aqueous Solution. *Langmuir* **2006**, *22*, 11022−11027.
(30) Hainfeld, J. F.; Slatkin, D. N.; Focella, T. M; Smilowitz, H. M. Gold Nanoparticles: a New X-ray Contrast Agent. *Br. J. Radiol.* **2006**, *79*, 248−253.
(31) Honda, K.; Kawazumi, H.; Nakashima, N.; Niidome, Y. Redispersion of Dried Gold Nanorods in the Presence of 6-Amino-1-Hexanethiol Hydrochloride. *J. Nanopart. Res.* **2011**, *13*, 3413−3421.
(32) Vigderman, L.; Manna, P.; Zubarev, E. R. Quantitative Replacement of Cetyl Trimethylammonium Bromide by Cationic Thiol Ligands on the Surface of Gold Nanorods and their Extremely Large Uptake by Cancer Cells. *Angew. Chem., Int. Ed.* **2012**, *51*, 636−641.
(33) Nikoobakht, B.; El-Sayed, M. A. Preparation and Growth Mechanism of Gold Nanorods (NRs) Using Seed-Mediated Growth Method. *Chem. Mater.* **2003**, *15*, 1957−1962.
(34) Khlebtsov, B.; Khanadeev, V.; Pylaev, T.; Khlebtsov, N. A New T-Matrix Solvable Model for Nanorods: TEM-Based Ensemble Simulations Supported by Experiments. *J. Phys. Chem. C* **2011**, *115*, 6317−6323.
(35) Frens, G. Controlled Nucleation for the Regulation of the Particle Size in Monodisperse Gold Suspensions. *Nat. Phys. Sci.* **1973**, *241*, 20−22.
(36) Skrabalak, S. E.; Au, L.; Li, X.; Xia, Y. Facile Synthesis of Ag Nanocubes and Au Nanocages. *Nat. Protoc.* **2007**, *2*, 2182−2190.
(37) Khlebtsov, B.; Panfilova, E.; Khanadeev, V.; Bibikova, O.; Terentyuk, G.; Ivanov, A.; Rumyantseva, V.; Shilov, I.; Ryabova, A.; Loshchenov, V.; Khlebtsov, N. Nanocomposites Containing Silica-Coated Gold−Silver Nanocages and Yb−2,4-Dimethoxyhematoporphyrin: Multifunctional Capability of IR-Luminescence Detection, Photosensitization, and Photothermolysis. *ACS Nano* **2011**, *5*, 7077−7089.
(38) Liao, H.; Hafner, J. H. Gold Nanorod Bioconjugates. *Chem. Mater.* **2005**, *17*, 4636−4641.
(39) http://conventions.coe.int/Treaty/en/Treaties/html/123.htm.
(40) Akiyama, Y.; Mori, T.; Katayama, Y.; Niidome, T. The Effects of PEG Grafting Level and Injection Dose on Gold Nanorod Biodistribution in the Tumor-Bearing Mice. *J. Controlled Release* **2009**, *139*, 81−84.
(41) Freund, Y. R.; Riccio, E. S.; Phillips, S. J.; Dousman, L.; MacGregor, J. T. Pyrimethamine Impairs Host Resistance to Infection with Listeria Monocytogenes in BALB/c Mice. *Toxicol. Sci.* **1998**, *42*, 91−98.
(42) Niidome, T.; Akiyama, Y.; Yamagata, M.; Kawano, T.; Mori, T.; Niidome, Y.; Katayama, Y. Poly(Ethylene Glycol)-Modified Gold Nanorods as a Photothermal Nanodevice for Hyperthermia. *J. Biomater. Sci., Polym. Ed.* **2009**, *20*, 1203−1215.
(43) Skirtach, A. G.; Dejugnat, Ch.; Braun, D.; Susha, A. S.; Rogach, A. L.; Parak, W. J.; Möhwald, H; Sukhorukov, G. B. The Role of Metal Nanoparticles in Remote Release of Encapsulated Materials. *Nano Lett.* **2005**, *5*, 1371−1377.
(44) Terentyuk, G. S.; Ivanov, A. V.; Polyanskaya, N. I.; Maksimova, I. L.; Skaptsov, A. A.; Chumakov, D. S.; Khlebtsov, B. N.; Khlebtsov, N. G. Photothermal Effects During the Laser Heating of Gold Nanorods in Suspensions and in Xenografted Tumors *in Vivo*. *Quantum Electron.* **2012**, *42* (in press).
(45) Habash, R. W.; Bansal, R.; Krewski, D.; Alhafid, H. T. Thermal Therapy, Part III: Ablation Techniques. *Crit. Rev. Biomed. Eng.* **2007**, *35*, 37−121.
(46) Goldberg, S. N.; Gazelle, G. S.; Mueller, P. R. Thermal Ablation Therapy for Focal Malignancy. *Am. J. Roentgenol.* **2000**, *174*, 323−331.
(47) Lapotko, D. Therapy with Gold Nanoparticles and Lasers: What Really Kills the Cells? *Nanomedicine (London, U.K.)* **2009**, *4*, 253−256.
(48) Hleb, E.; Hu, Y.; Drezek, R.; Hafner, J.; Lapotko, D. Photothermal Bubbles as Optical Scattering Probes for Imaging Living Cells. *Nanomedicine (London, U.K.)* **2008**, *3*, 797−812.
(49) Lapotko, D.; Lukianova, E.; Potapnev, M.; Aleinikova, O.; Oraevsky, A. Method of Laser Activated Nano-Thermolysis for Elimination of Tumor Cells. *Cancer Lett.* **2005**, *239*, 36−45.
(50) Zharov, V. P.; Galitovskaya, E. N.; Johnson, C.; Kelly, T. Synergistic Enhancement of Selective Nanophotothermolysis with Gold Nanoclusters: Potential for Cancer Therapy. *Lasers Surg. Med.* **2005**, *37*, 219−226.
(51) Diagaradjane, P.; Shetty, A.; Wang, J. C.; Elliott, A. M.; Schwartz, J.; Shentu, S.; Park, H. C.; Deorukhkar, A.; Stafford, R. J.; Cho, S. H.; Tunnell, J. W.; Hazle, J. D.; Krishnan, S. Modulation of *in Vivo* Tumor Radiation Response via Gold Nanoshell-Mediated Vascular-Focused Hyperthermia: Characterizing an Integrated Anti-hypoxic and Localized Vascular Disrupting Targeting Strategy. *Nano Lett.* **2008**, *8*, 1492−1500.
(52) Goel, R.; Shah, N.; Visaria, R.; Paciotti, G. F.; Bischof, J. C. Biodistribution of TNF-$\alpha$-Coated Gold Nanoparticles in an *in Vivo* Model System. *Nanomedicine (London, U.K.)* **2009**, *4*, 401−410.
(53) Dreaden, E. C.; Mackey, M. A.; Huang, X.; Kangy, B.; El-Sayed, M. A. Beating Cancer in Multiple Ways Using Nanogold. *Chem. Soc. Rev.* **2011**, *40*, 3391−3404.
(54) Farma, J. M.; Puhlmann, M.; Soriano, P. A.; Cox, D.; Paciotti, G. F.; Tamarkin, L.; Alexander, H. R. Direct Evidence for Rapid and Selective Induction of Tumor Neovascular Permeability by Tumor Necrosis Factor and a Novel Derivative, Colloidal Gold Bound Tumor Necrosis Factor. *Int. J. Cancer* **2007**, *120*, 2474−2480.
(55) Libutti, S. K.; Paciotti, G. F.; Myer, L.; Haynes, R.; Gannon, W. E.; Eugeni, M.; Seidel, G.; Shutack, Y.; Yuldasheva, N.; Tamarkin, L. Preliminary Results of a Phase I Clinical Trial of CYT-6091: a Pegylated Colloidal Gold-TNF Nanomedicine. *J. Clin. Oncol.* **2007**, *25*, 3603.

# Supporting Information

# Plasmonic nanopowders for photothermal therapy of tumors

Boris N. Khlebtsov[a], Elizaveta V. Panfilova[a], Georgy S. Terentyuk[b], Andrey V. Ivanov[c], Irina L. Maksimova[b] and Nikolai G. Khlebtsov[a,b,*]

[a]Institute of Biochemistry and Physiology of Plants and Microorganisms, Russian Academy of Sciences,

13 Prospekt Entuziastov, Saratov 410049, Russia, e-mail: khlebtsov@ibppm.sgu.ru

[b]Saratov State University, 83 Ulitsa Astrakhanskaya, Saratov 410026, Russia

[c]Blokhin Russian Cancer Research Center, 24 Kashirskoe Shosse, Moscow 115478, Russia

## S1. Extinction spectra of CTAB-coated GNRs before and after freeze-drying

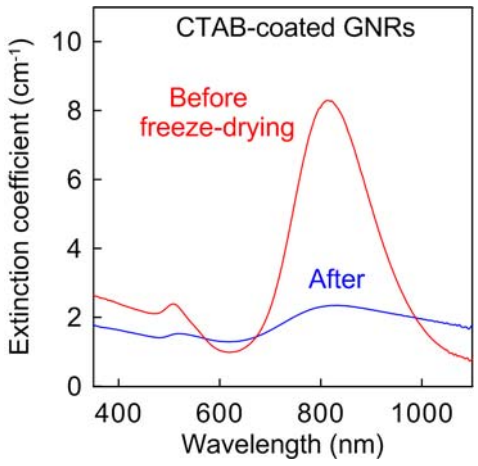


**Figure S1**. Extinction spectra of as-prepared CTAB-coated GNRs and those after freeze-drying, redispersion in water, and sonication.

## S2. TEM images of CTAB- and PEG-coated GNRs before and after freeze-drying

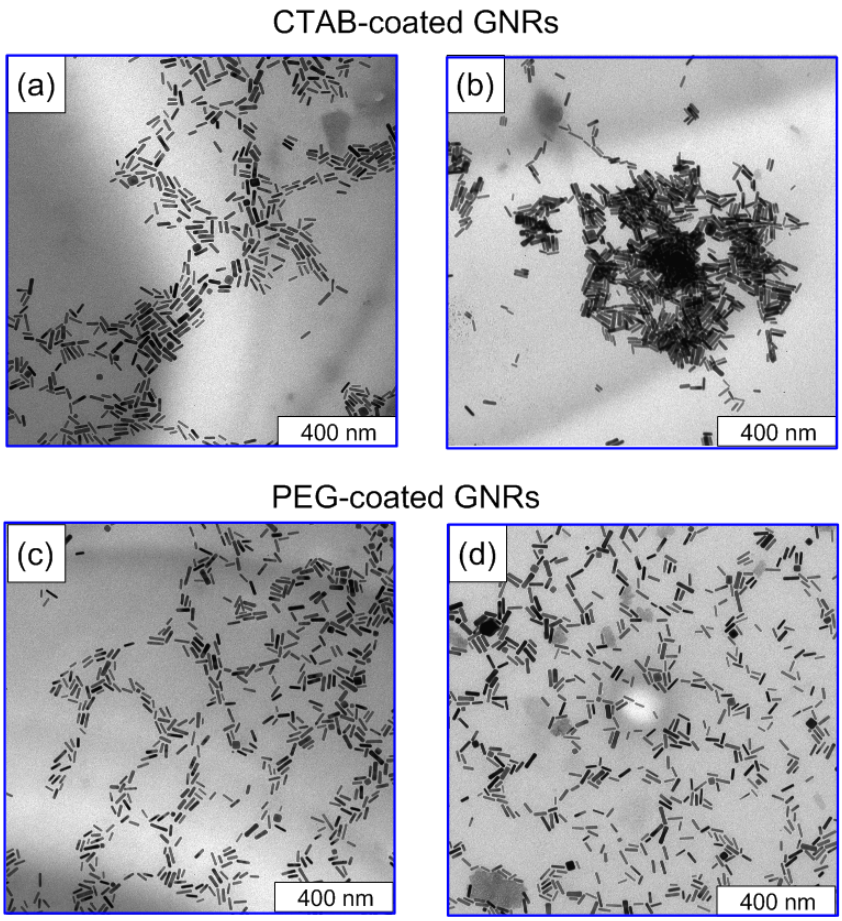


**Figure S2**. TEM images of CTAB-coated (a, b) and PEG-coated (c, d) GNRs before (a, c) and after (b, d) freeze-drying and redispersion in water.

**S3. Fabrication of silver nanocubes**. Au–Ag nanocages were prepared by a two-step process previously reported by Skrabalak *et al.*,[1] with a minor modification.[2] In the first step, Ag nanocube templates were prepared. Briefly, 30 mL of ethylene glycol was added to a 250-mL round-bottomed flask and was heated in an oil bath at 150 °C under magnetic stirring. After 50-min preheating, a flow of argon was introduced at a rate of 1200 mL/min. Ten min after, a sodium sulfide solution in EG (0.35 mL, 3 mM) was quickly injected into the preheated EG solution, followed by injection of a PVP solution in EG (7.5 mL, 20 g/L) and 8 min later by injection of a silver nitrate solution in EG (2.5 mL, 48 g/L). Shortly after the addition of $AgNO_3$, the reaction solution went through four distinct stages of color change, from golden yellow to deep red, reddish gray, and then green ocher within about 30 min. The reaction solution was then quenched by placing the reaction flask in an ice-water bath. The resultant product was washed by

centrifugation (12000 g, 30 min) and was redispersed in acetone, followed by redispersion in ethanol to remove excess EG and PVP. Finally, the Ag nanocubes were redispersed in 40 mL of ethanol. In a typical synthesis, the product contained 0.05 g of solid Ag, corresponding to cubic nanoparticles with an average edge length of 43 ± 5 nm, a number concentration of $1.4\times10^{15}$ $L^{-1}$, and an extinction coefficient of about 370 $cm^{-1}$ at 454 nm (the resonance optical density of a 1:50 diluted suspension in a 2-mm cuvette equals 0.64).

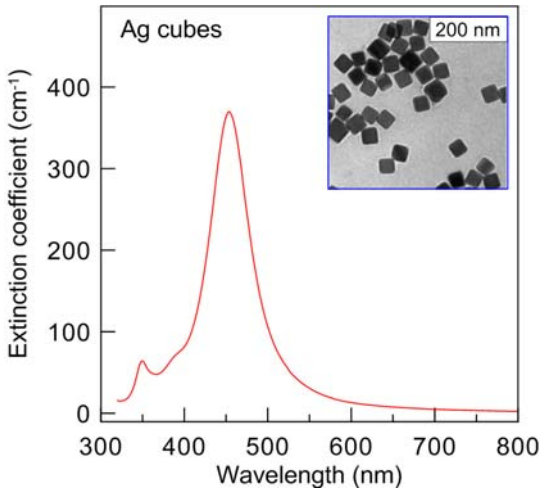


**Figure S3**. Extinction spectrum and TEM image of as-prepared silver nanocubes.

**S4. Fabrication of Au–Ag nanocages**. The isolated Ag nanocubes were converted into Au–Ag nanocages *via* the galvanic replacement reaction.[1] Briefly, a PVP water solution (100 mL, 1 g/L) was heated at 100 $^0$C under magnetic stirring, followed by injection of 2 mL of the as-prepared nanocubes suspension in ethanol. Three min after, 10 mL of a 1mM $HAuCl_4$ solution was added drop by drop during 10 min. The addition of $HAuCl_4$ to the reaction mixture was accompanied by four distinct changes in color, from orange yellow to deep red, purple, and finally light blue. The appearance of a light blue color indicates the successful formation of Au nanocages owing to the galvanic replacement reaction between solid Ag and $Au^{3+}$ ions. The reaction solution was then quenched by placing the reaction flask in an ice-water bath. This was followed by the addition of $NH_4OH$ (0.7 mL, 30% wt) to dissolve solid AgCl formed as a byproduct. The nanocages were washed by centrifugation (12000 g, 20 min) and were redispersed in water three times. Finally, the Au–Ag nanocages were redispersed in 100 mL of

water. In a typical synthesis, the product contained nanocages with an average edge length of about (45–50) ± 5 nm and an extinction coefficient of about 3.5 $cm^{-1}$ at resonance wavelength near 745 nm, depending on the Ag/Au conversion ratio. The predicted concentrations of Ag and Au are 8 mg/L and 15 mg/L, respectively.

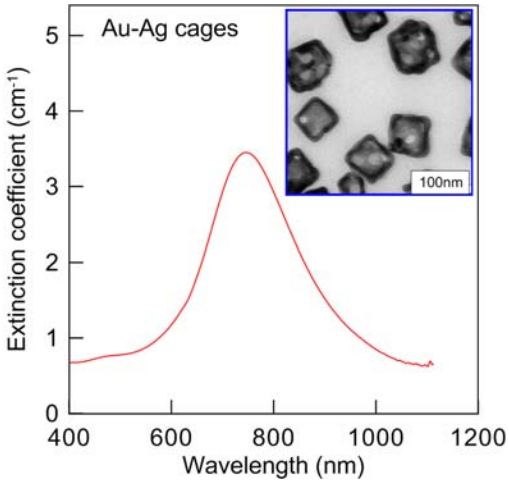


**Figure S4**. Extinction spectrum and TEM image of as-prepared Au–Ag nanocages.

**S5. Synthesis of 56-nm colloidal gold particles**

Fifty-nm colloidal gold nanoparticles were prepared by citrate reduction of $HAuCl_4$[3]. Briefly, 100 mL of water was boiled in an Erlenmeyer flask fitted with a reflux condenser, on a magnetic stirrer for 20 min. Then, 1 mL of 1% aqueous $HAuCl_4$ and 0.88 mL of sodium citrate (10 mg/mL) were added sequentially. This resulted in the formation of colloidal gold particles of quasispherical shape at a total mass-volume concentration of 57 mg/L. The extinction coefficient of this colloid was about 2.9 $cm^{-1}$ at 530 nm (Fig. 5S).

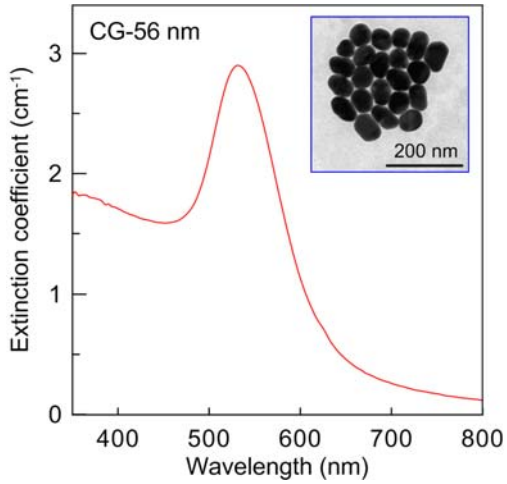


**Figure 5S**. Extinction spectrum and TEM image of 56-nm colloidal gold nanoparticles.

## S6. Implanted Ehrlich carcinoma tumor image


**Figure 6S**. Ehrlich carcinoma tumor at 14 days after implantation.

## S7. Toxicity of PEG-coated GNRs after freeze-drying

To evaluate the toxicity of PEG-coated GNRs after freeze-drying, we examined the viability of HeLa cells (MTT assay) at GNR concentrations ranging from 1 to 100 mg/L. HeLa cells (Saratov Science Research Veterinary Station, Saratov, Russia) were maintained at 37 $^{o}$C and 5% $CO_2$ in complete DMEM medium (Biolot Co., Russia) supplemented with 10% bovine serum, 300 mg/L L-glutamine, 100 mg/L ampicillin, 50 mg/L gentamicin, and 2.5 mg/L amphotercin B (all from Biolot). The cell suspension was centrifuged at 1000 g for 5 min and then was redispersed in Hanks' solution (Biolot). One mL of the cell suspension ($10^8$ cells/L) was incubated with 0.2 mL of free GNR solutions for 24 h. Cell viability was measured by the MTT assay.[4] In brief, after incubation with GNRs, the cells were centrifuged at 1000 g for 5 min, redispersed in 0.5 mL of MTT solution (Sigma, USA), and incubated for 1 h in the dark at 37º C. Then, the cells were centrifuged at 1000 g for 5 min and were redispersed in 0.5 mL of DMSO (ASC Grade DMSO, Amresco, USA) to dissolve formazan crystals. The samples were centrifuged at 12,000 g for 5 min in 1.5 mL Eppendorf tubes (Eppendorf Minispin), and 0.2 mL of the supernatant liquids was transferred to 96-well plates. Absorbance values at 492 nm were collected on a Multiskan Ascent microplate reader (Thermo Fisher Scientific Inc).

Figure 7S shows that no toxicity of freeze-dried GNRs was observed for all concentrations in the range 1–100 mg/L. The somewhat enhanced MTT activity of the treated cells can be

attributed to experimental errors, and the differences between control and experimental data are within statistical tolerance.

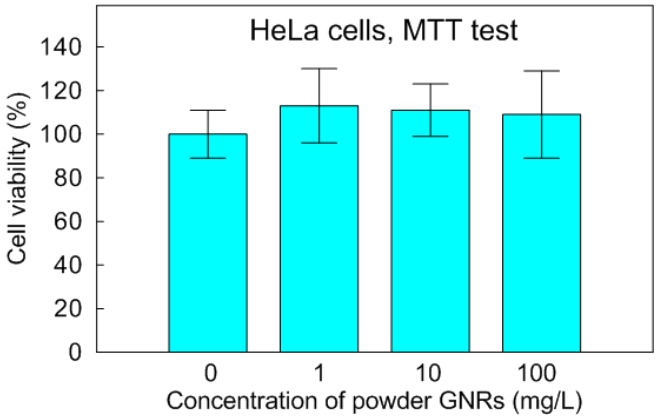


**Figure 7S**. MTT assay for redispersed freeze-dried GNRs by using HeLa cells.

**S8. Video file**

The video file "GNR-PEG-SH-Powder.wmv" illustrates convenient work with the fabricated powder including, its transfer from the storage vessel for weighing, redispersion in water, and spectral measurements.

## References

1. Skrabalak, S. E.; Au, L.; Li, X.; Xia, Y. Facile Synthesis of Ag Nanocubes and Au Nanocages. *Nat. Protoc*. **2007**, *2*, 2182–2190

2. Khlebtsov, B.; Panfilova, E.; Khanadeev, V.; Bibikova, O.; Terentyuk, G.; Ivanov, A.; Rumyantseva, V.; Shilov, I.; Ryabova, A.; Loshchenov, V.; Khlebtsov, N. Nanocomposites Containing Silica-Coated Gold–Silver Nanocages and Yb–2,4-Dimethoxyhematoporphyrin: Multifunctional Capability of IR-Luminescence Detection, Photosensitization, and Photothermolysis. *ACS Nano* **2011**, *5*, 7077–7089.

3. Frens, G. Controlled Nucleation for the Regulation of the Particle Size in Monodisperse Gold Suspensions. *Nature Phys. Sci.* **1973**, *241*, 20–22.

4. Oez, S; Platzer, E.; Welte, K. A. A Quantitative Colorimetric Method to Evaluate the Functional State of Human Polymorphonuclear Leukocytes. *Blut* **1990**, *60*, 97–102.